



MOX-Report No. 08/2015

**Numerical simulation of geochemical compaction with  
discontinuous reactions**

Agosti, A.; Formaggia, L.; Giovanardi, B.; Scotti, A.

MOX, Dipartimento di Matematica  
Politecnico di Milano, Via Bonardi 9 - 20133 Milano (Italy)

[mox-dmat@polimi.it](mailto:mox-dmat@polimi.it)

<http://mox.polimi.it>

# Numerical simulation of geochemical compaction with discontinuous reactions

ABRAMO AGOSTI<sup>#</sup>, LUCA FORMAGGIA<sup>#</sup>,  
BIANCA GIOVANARDI<sup>#</sup>, and ANNA SCOTTI<sup>#</sup>

February 2, 2015

<sup>#</sup> MOX– Modellistica e Calcolo Scientifico  
Dipartimento di Matematica “F. Brioschi”  
Politecnico di Milano  
via Bonardi 9, 20133 Milano, Italy  
abramo.agosti@polimi.it  
luca.formaggia@polimi.it  
bianca.giovanardi@polimi.it  
anna.scotti@polimi.it

**Keywords:** compaction processes, discontinuous RHS ODE, mineral dissolution/precipitation.

## Abstract

The present work deals with the numerical simulation of porous media subject to the coupled effects of mechanical compaction and reactive flows that can significantly alter the porosity due to dissolution, precipitation or transformation of the solid matrix. These chemical processes can be effectively modelled by ODEs with discontinuous right hand side, where the discontinuity depends on time and on the solution itself. Filippov theory can be applied to prove existence and to determine the solution behaviour at the discontinuities. From the numerical point of view, tailored numerical schemes are needed to guarantee positivity, mass conservation and accuracy. In particular, we rely on an event-driven approach such that, if the trajectory crosses a discontinuity, the transition point is localized exactly and integration is restarted accordingly.

## 1 Introduction

We propose a model to describe and simulate the compaction process under a progressive burial of a layer of sediments in which a mineral can dissolve in the water flow and precipitate on the grains of the rock. On one hand, compaction is due to the burial of the layer, which makes the overburden increase. On the other, the presence of the precipitated mineral can affect the solid matrix porosity, since the dissolving mineral may leave some void spaces, whereas the precipitating mineral may fill them. Moreover,

an alteration of porosity implies a variation of permeability that affects the pressure of the water flowing through the rock layer. Again, the fluid pressure counteracts compaction reducing the effective vertical stress, which has an effect on porosity. Finally, the chemical reactions that cause the mineral to dissolve and precipitate are influenced by the fluid flow, which transports the solute.

The result is a nonlinear system of strongly coupled equations. The flow is assumed to obey Darcy's law. We use a simplified description of chemical reactions to model the precipitation and dissolution of a mineral, such as quartz, see [2, 7, 10]. The effect of the fluid-solid conversion on porosity is accounted for by modifying Athy's constitutive law for the porosity [1], following [15, 16]. Again, we follow the strategy proposed in [15] and recast the governing equations in a Lagrangian frame. We simulate the sedimentation process by providing a sedimentation rate that cause the overburden to increase.

The system is solved by splitting the stronger coupling between pressure and compaction from the solution of the advection-diffusion-reaction equation for the transported solute. One main issue is that the equation that models the reaction of the mineral is a differential equation with discontinuous right hand side [9]. This led us to introduce another splitting between the advection-diffusion part of this equation and the reaction one, to take advantage of the available *ad hoc* methods to manage the discontinuity. In particular, among the possible strategies such as time step adaptation, [8], or regularization of the right hand side, [4], we chose to adopt an event-driven approach where the crossing of the discontinuity is exactly localized before restarting integration [5].

The paper is structured as follows. In Section 2 we present the mathematical model and we recast it into a Lagrangian frame. Section 3 deals with the numerical approach. In particular, we dwell on the application of a method to treat ODEs with discontinuous right hand side to our specific case. Finally in Section 4 the numerical solution obtained in three test configurations are analyzed, while conclusions are drawn in Section 5.

## 2 The model

We consider a layer of a sedimentary rock subject to a progressive burial. We assume that the porous medium is saturated with water. We are interested in modeling the behavior of a reactive material that can be advected by the flow when dissolved in water, and precipitate on the grains surface in the rocks. On the other hand, the precipitated mineral may dissolve into the fluid. It is clear that this mechanism, together with the increasing load due to the burial of the layer, affects the porosity  $\phi$  of the sediments, leading to both geochemical and mechanical compaction.

### 2.1 The domain

We consider a two-dimensional model of the aforementioned processes, simulated in a vertical cross section of the sedimentary layer. Due to compaction, the domain of interest  $\Omega$ , evolves during the simulation. However, it is more convenient to cast the

coupled problem of fluid flow, compaction and chemical reactions in a fixed geometry. For this reason, under the assumption that compaction acts only vertically, we define a fixed domain  $\hat{\Omega}$ , obtained from  $\Omega = \Omega(t)$ , as its completely compacted configuration once removed the reactive (dissolvable) part of the rock, as sketched in figure 1.

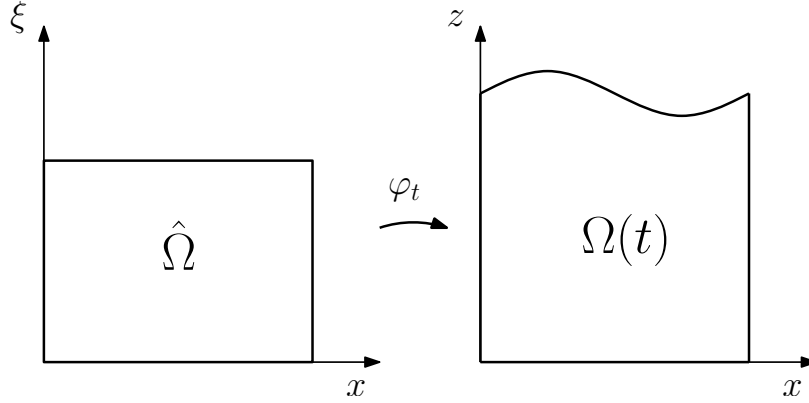


Figure 1: A sketch of the two domains involved.  $\Omega(t)$  is the physical domain and  $\hat{\Omega}$  is not time-dependent.

More precisely, following [15] and [16], we assume that one can define at any point  $\mathbf{x} \in \Omega(t)$  and at any time the field  $C = C(\mathbf{x}, t)$ , which represents the ratio between the volume of the reactive part of the rock and the initial rock volume, so that the map  $\varphi_t : \hat{\Omega} \rightarrow \Omega(t)$ ,  $(x, \xi) \mapsto (x, z(\xi, t))$ , is

$$\varphi_t(x, \xi) = \left( x, z_{top}(x, t) - \int_{\xi}^{\xi^*(x)} \frac{1 - C_0(x, \xi') + C(x, \xi', t)}{(1 - C_0(x, \xi'))(1 - \phi(x, \xi', t))} d\xi' \right), \quad (1)$$

where  $\xi^*(x)$  is the thickness of the layer along the  $\xi$ -axis, which is constant,  $z_{top}$  is the thickness of the layer along the  $z$ -axis and is time-dependent, and  $C_0(x, \xi') = C(x, \xi', 0)$ .

The deformation gradient  $\mathbf{F}$  associated to this map is

$$\mathbf{F} := \nabla \varphi_t = \begin{bmatrix} 1 & 0 \\ \partial z / \partial x & \partial z / \partial \xi \end{bmatrix}, \quad (2)$$

and the Jacobian reads

$$J := \det(\mathbf{F}) = \frac{\partial z}{\partial \xi} = \frac{1 - C_0 + C}{(1 - C_0)(1 - \phi)} > 0. \quad (3)$$

Note that the time derivative of the map coincides with the velocity  $\mathbf{u}_s$  of the sediments and that, due to the hypothesis of vertical compaction,  $\mathbf{u}_s = u_{sz} \mathbf{e}_z$ , being  $\mathbf{e}_z$  the unit vector of the  $z$ -axis.

## 2.2 Governing equations

In this section we present the equations governing the porous matrix evolution, fluid flow and chemical reactions in the physical, thus time dependent, domain  $\Omega(t)$ .

In this framework, mass conservation of the solid phase in a porous medium implies

$$\frac{\partial}{\partial t} ((1 - \phi)\rho_s) + \frac{\partial}{\partial z} ((1 - \phi)\rho_s u_{sz}) = Q_s \quad \text{in } \Omega(t) \times (0, T), \quad (4)$$

where  $Q_s$  is a source/sink term that models the growth or consumption of the solid grains. The density  $\rho_s$  of the solid matrix is obtained as the average of the density of the inert part of the rock  $\rho_r$  and that of the precipitated mineral  $\rho_p$ , weighted with their volume fractions, that is

$$\rho_s = \frac{(1 - C_0)\rho_r + C\rho_p}{1 - C_0 + C}. \quad (5)$$

If we assume that no water is released or consumed during the reactions, mass conservation for the fluid phase reads

$$\frac{\partial}{\partial t} (\phi\rho_w) + \nabla \cdot (\phi\rho_w \mathbf{u}_w) = 0 \quad \text{in } \Omega(t) \times (0, T), \quad (6)$$

where  $\rho_w$  is the density of water and  $\mathbf{u}_w$  its macroscopic velocity.

The relative velocity of the water with respect to the solid matrix is related to the pore pressure  $p$  by Darcy's law, i.e.

$$\phi(\mathbf{u}_w - \mathbf{u}_s) = -\frac{\mathbf{K}}{\mu_w} (\nabla p - \rho_w \mathbf{g}) \quad \text{in } \Omega(t) \times (0, T), \quad (7)$$

with  $\mathbf{g} = -g\mathbf{e}_z$ .  $\mu_w$  denotes the water viscosity and  $\mathbf{K}$  is the permeability tensor, which we assume to be isotropic, thus

$$\mathbf{K}(\phi) = \mathcal{K}(\phi)\mathbf{I} \quad (8)$$

being  $\mathcal{K}(\phi)$  given by the following relation, see [3],

$$\mathcal{K}(\phi) = \begin{cases} k_0\phi^3 & \text{if } \phi \geq 0.1 \\ \frac{100 k_0\phi^5}{(1 - \phi)^2} & \text{if } \phi < 0.1 \end{cases}. \quad (9)$$

Mechanical compaction of porous media is usually modeled by a relation between porosity and effective vertical stress known as Athy's law, [1]. However, in the case of our interest, porosity depends also on the concentration of precipitated mineral  $C$ . According to [15], we model the coupled effect of dissolution/precipitation and compaction with the following equation,

$$\phi = (\phi_0 + (1 - \phi_0)(C_0 - C)) e^{-\beta \sigma}, \quad (10)$$

which is a generalization of Athy's law. Here,  $\sigma$  denotes the vertical effective stress defined as  $\sigma = s - p$ , where  $s$  is the overburden and can be obtained integrating the differential equation

$$\frac{\partial s}{\partial z} = -[(1 - \phi)\rho_s + \phi\rho_f] g \quad (11)$$

with the boundary condition  $s(x, z_{top}, t) = s_{top}(t)$ , where  $s_{top}$  is a given function of time and accounts for the weight of the overlying layers. The equations (4), (6), (11) describe the coupling between water flow and compaction. We now introduce the chemical reactions that model the precipitation and dissolution of the transported mineral specie. Let us introduce the field  $\gamma$  that represents the dissolved mineral concentration in terms of moles per unit volume of water. The dissolved mineral is allowed to diffuse, to be transported by the fluid flow and to interact with the solid matrix, i.e. to precipitate, behaving as prescribed by the following equation:

$$\frac{\partial}{\partial t}(\gamma\phi) + \nabla \cdot (\phi\gamma(\mathbf{u}_w - \mathbf{u}_s) - D\phi\nabla\gamma) = r(C, \gamma)\phi \quad \text{in } \Omega(t) \times (0, T), \quad (12)$$

where  $D > 0$  is the diffusion coefficient and  $r(C, \gamma)$  is a source/well term that represents the dissolution/precipitation rate of the mineral. We point out that, since we are considering low velocities we are here neglecting the effect of dispersion.

On the other hand, a source/sink term for equation (12) implies a sink/source term for the equation of the volume fraction of the precipitated mineral, as stated by the following equation:

$$\frac{\partial C}{\partial t} = -V_m r(C, \gamma)\phi, \quad (13)$$

where  $V_m$  is the molar volume of the mineral.

Following [2], we model the reaction rate  $r$  as a discontinuous function of  $\gamma$  and  $C$ . Let us introduce the following notation

$$x^+ := \max(0, x), \quad x^- := (-x)^+.$$

We model the source/sink term for the equations (12) and (13) as

$$r(C, \gamma) = \lambda (\text{sign}(C)^+ F(\gamma)^- - F(\gamma)^+), \quad (14)$$

where

$$F(\gamma) = \frac{\gamma}{\gamma_{eq}} - 1, \quad \gamma_{eq} > 0.$$

Here,  $\gamma_{eq}$  denotes an equilibrium concentration of the dissolved mineral. The rate constant  $\lambda$  is modeled according to Arrhenius law as

$$\lambda = \bar{\lambda} e^{-\frac{E}{RT}} > 0,$$

where  $E$  is an activation energy,  $R$  is the gas constant and the temperature  $T$  is assumed to be a given function of time.

We observe that, if the solute concentration exceeds the equilibrium value,  $\gamma > \gamma_{eq}$ , then  $F(\gamma) > 0$  and  $r = -\lambda \left( \frac{\gamma}{\gamma_{eq}} - 1 \right) < 0$ . In this case, precipitation occurs. On the other hand, if  $\gamma < \gamma_{eq}$ , then  $F(\gamma) < 0$  and  $r = \lambda \text{sign}(C)^+ \left( 1 - \frac{\gamma}{\gamma_{eq}} \right) \geq 0$ . In this case, if  $\text{sign}(C) > 0$  (i.e. if some precipitated is available in the rock), dissolution occurs. Finally, in case  $\gamma = \gamma_{eq}$ ,  $F(\gamma) = 0$  and the chemical equilibrium implies  $r = 0$ .

### 2.3 The equations in $\hat{\Omega} \times (0, T)$

As we have anticipated, the physical domain  $\Omega(t)$  is time dependent. For this reason, it is convenient to solve the problem numerically in the artificial fixed domain  $\hat{\Omega}$ . The generic scalar field in  $\Omega$  becomes  $\hat{f} = f \circ \varphi_t$  in  $\hat{\Omega}$ , and the generic vector field  $\mathbf{v}$  is transformed through the Piola transformation, that is  $\hat{\mathbf{v}} = \hat{J} \hat{\mathbf{F}}^{-1} \mathbf{v} \circ \varphi_t$ , where  $\hat{J}$  and  $\hat{\mathbf{F}}$  are the transformation of (2) and (3). Finally, the nabla operator in the fixed coordinate system becomes

$$\hat{\nabla} = \begin{pmatrix} \partial/\partial x \\ \partial/\partial \xi \end{pmatrix} = \hat{\mathbf{F}} \nabla = \hat{\mathbf{F}} \begin{pmatrix} \partial/\partial x \\ \partial/\partial z \end{pmatrix}.$$

Since, as observed before, the time derivative of the map is the velocity  $\mathbf{u}_s$  of the solid matrix, equation (4) reformulated in  $\hat{\Omega} \times (0, T)$  simplifies and becomes

$$\frac{\partial}{\partial t} \left( (1 - \hat{\phi}) \hat{\rho}_s \hat{J} \right) = \hat{Q}_s \hat{J}. \quad (15)$$

Inserting (3) and (5) into (15) and developing the time derivative, the following expression for  $\hat{Q}_s$  can be obtained:

$$\hat{Q}_s = \rho_p \frac{(1 - \hat{\phi})}{1 - \hat{C}_0 + \hat{C}} \frac{\partial \hat{C}}{\partial t}. \quad (16)$$

The solid mass conservation equation (4), completed with the right hand side (16), allows us to compute, knowing porosity and precipitate concentration, the velocity of the solid matrix and therefore the deformed configuration of the layer. Indeed, one can solve (4) for  $u_{sz}$  with a Dirichlet condition on the bottom boundary, and solve then  $\frac{\partial z}{\partial t} = u_{sz}$  with a proper initial condition. We point out that, since we are considering the evolution of a single layer, such boundary conditions should be provided by the reconstruction of the history of the whole sedimentary basin.

Equations (6), (7), (10), and (11) can be cast on  $\hat{\Omega} \times (0, T)$  as

$$\begin{cases} \frac{\partial(\hat{\phi} \hat{\rho}_w \hat{J})}{\partial t} + \hat{\nabla} \cdot (\hat{\phi} \hat{\rho}_w \hat{\mathbf{u}}) = 0 \\ \hat{\phi} \hat{\mathbf{u}} = -\hat{J} \frac{\tilde{\mathbf{K}}}{\mu_w} \left( \hat{\nabla} \hat{p} - \hat{\rho}_w \hat{\mathbf{F}}^T \hat{\mathbf{g}} \right) \\ \hat{\phi} = (\phi_0 + (1 - \phi_0)(\hat{C}_0 - \hat{C})) e^{-\beta(\hat{s} - \hat{p})} \\ \frac{\partial \hat{s}}{\partial \xi} = -[(1 - \hat{\phi}) \hat{\rho}_s + \hat{\phi} \hat{\rho}_f] \hat{g} \hat{J} \end{cases}, \quad (17)$$

where we have set  $\tilde{\mathbf{K}} := \hat{\mathbf{F}}^{-1} \mathbf{K}(\hat{\phi}) \hat{\mathbf{F}}^{-T}$ , and  $\hat{\mathbf{u}} = \hat{\mathbf{u}}_w - \hat{\mathbf{u}}_s$ .

Finally, the equations for the concentration of the transported mineral and for the volume fraction of the precipitated on the solid matrix, in the fixed domain, are

$$\begin{cases} \frac{\partial}{\partial t}(\hat{\gamma} \hat{\phi} \hat{J}) + \hat{\nabla} \cdot (\hat{\phi} \hat{\gamma} \hat{\mathbf{u}} - D \hat{\phi} \hat{\mathbf{F}}^{-T} \hat{\nabla} \hat{\gamma}) = \hat{r}(\hat{C}, \hat{\gamma}) \hat{\phi} \hat{J} \\ \frac{\partial \hat{C}}{\partial t} = -V_m \hat{r}(\hat{C}, \hat{\gamma}) \hat{\phi}. \end{cases} \quad (18)$$

The system formed by equations (17) and (18), complemented with suitable initial and boundary conditions, is a nonlinear system of strongly coupled equations. Indeed, it is clear that the changes in porosity can cause overpressures (i.e. pressures larger than hydrostatic) because permeability is a function of porosity, and moreover porosity plays a role in the storage term of fluid mass conservation. On the other hand, fluid pressure can counteract compaction reducing the effective vertical stress. Finally, chemical reactions are influenced by the fluid flow which transports the solute, and can increase or reduce the porosity if dissolution or precipitation occur. The approximation strategy implemented to tackle this coupling is illustrated in the next section.

### 3 The numerical approximation

For the solution of the coupled problem described in the previous section one could opt for a fully coupled approach using Newton iterations. However, even if a fully coupled approach is in general more robust, it is computationally very expensive and moreover the Jacobian matrix is likely to be ill-conditioned because of the different scales involved in the equations. For this reason we resort to an iterative splitting where the problems are solved in sequence, performing fixed point iterations until convergence is achieved.

#### 3.1 Time discretization and iterative splitting

In principle all the aforementioned problems, i.e. fluid flow, compaction and solute dissolution/precipitation are coupled. If we assume that the effect of chemistry on porosity is moderate and relatively "slow" we can solve via fixed point iterations only the stronger coupling between pressure and compaction, and solve the advection, diffusion and reaction for the solute once per time step, reducing the computational cost. Therefore, for each time, we are performing the following steps:

- integrate (18)
- enter the fixed point loop
  - compute the sedimentary load and the effective stress
  - update of the porosity
  - solve Darcy's problem, to obtain fluid pressure

– check for convergence.

Since the reaction term in the ADR equation for  $\gamma$  is discontinuous, its approximation can benefit from a tailored integration scheme. Therefore it is very convenient, though not mandatory, to split the equation into an advection-diffusion part and a reaction part. This way, starting from the coupled problem (18) we can split it into two sub-problems:

#### Advection-diffusion equation

$$\frac{\partial}{\partial t}(\hat{\gamma}\hat{\phi}\hat{J}) + \hat{\nabla} \cdot (\hat{\phi}\hat{\gamma}\hat{\mathbf{u}} - D\hat{\phi}\hat{\mathbf{F}}^{-T}\hat{\nabla}\hat{\gamma}) = 0 \quad (19)$$

#### Reaction system

$$\begin{cases} \frac{\partial \hat{\gamma}}{\partial t} = \hat{r}(\hat{C}, \hat{\gamma}) \\ \frac{\partial \hat{C}}{\partial t} = -V_m \hat{r}(\hat{C}, \hat{\gamma}) \hat{\phi} \end{cases} \quad (20)$$

The two problems are solved in sequence according to a second order Strang splitting ([11,13]). If we denote with  $\hat{\gamma}^{n,n+1}$ ,  $\hat{C}^{n,n+1}$  the concentrations at the discrete time  $t^n$  and  $t^{n+1}$  respectively, with  $\hat{\gamma}^{*,**}$  two intermediate values of  $\hat{\gamma}$  and with  $\Delta t$  the time step amplitude, the splitting consists in performing the following three steps

$$\begin{aligned} I) & \frac{2(\hat{\gamma}^*\hat{\phi}\hat{J} - \hat{\gamma}^n\hat{\phi}\hat{J})}{\Delta t} + \hat{\nabla} \cdot (\hat{\phi}\hat{\gamma}^*\hat{\mathbf{u}} - D\hat{\phi}\hat{\mathbf{F}}^{-T}\hat{\nabla}\hat{\gamma}^*) = 0 \\ II) & \begin{cases} \frac{\hat{\gamma}^{**} - \hat{\gamma}^*}{\Delta t} = \hat{r}(\hat{C}^n, \hat{\gamma}^*) \\ \frac{\hat{C}^{n+1} - \hat{C}^n}{\Delta t} = -V_m \hat{r}(\hat{C}^n, \hat{\gamma}^*) \hat{\phi} \end{cases} \\ III) & \frac{2(\hat{\gamma}^{n+1}\hat{\phi}\hat{J} - \hat{\gamma}^{**}\hat{\phi}\hat{J})}{\Delta t} + \hat{\nabla} \cdot (\hat{\phi}\hat{\gamma}^{n+1}\hat{\mathbf{u}} - D\hat{\phi}\hat{\mathbf{F}}^{-T}\hat{\nabla}\hat{\gamma}^{n+1}) = 0. \end{aligned}$$

Note that we have chosen an implicit, thus more stable, discretization for the advection-diffusion part, while as concerns the reaction part an explicit scheme is more suitable for the implementation of the event detection method described in section 3.3. We also point out that we are employing a higher order splitting to achieve better accuracy. Since for each time step we also need to solve some fixed point iterations for pressure and porosity, the use of an higher order splitting turns out to be to be more efficient than using a smaller the time step.

### 3.2 Finite element discretization

We have chosen a mixed finite element method for both the Darcy's problem and the advection-diffusion part of the equation for the solute concentration. This allows us to

use the same finite element approximation for the relative velocity  $\hat{\mathbf{u}}$  in equations (19) and (17,1). The finite element space chosen for the relative velocity  $\hat{\mathbf{u}}$  is the lowest order Raviart Thomas  $\mathbb{RT}_0(\hat{\Omega}, \mathcal{T}_h) \subset H(\text{div}, \hat{\Omega})$ , while the solute concentration  $\gamma$  and the water pressure  $p$  are in the space of the piece-wise constant functions  $\mathbb{P}_0(\hat{\Omega}, \mathcal{T}_h) \subset L^2(\hat{\Omega})$ . In both equations, since we are considering mixed formulations, the Dirichlet boundary conditions on pressure and concentration are naturally included in the weak formulation, while the Neumann boundary conditions on normal velocity and flux are imposed with a Nitsche's penalization technique (see [12]). Finally, the differential equation for the computation of the overburden  $s$  is solved with a SUPG stabilized finite element method, using  $\mathbb{P}_1$  elements.

### 3.3 Numerical solution of the discontinuous ODEs for dissolution/precipitation

We now focus on the numerical approximation of the reaction part of the coupled problem (18). Thanks to the splitting we can employ an *ad hoc* method for discontinuous ODEs. Indeed, once the problem has been discretized in space with the finite element method as described in the previous section, equations (20) become a system of ODEs for each single degree of freedom. If we denote as  $\hat{\gamma}$ ,  $\hat{C}$  the vectors containing the degrees of freedom representing the solute and precipitate concentrations, being  $\hat{\mathbf{r}}$  the corresponding vector of the reaction rates defined as in (14), (18) is an ODE system with discontinuous right hand side, to whom Filippov theory can be applied. To this purpose, we define

$$\mathbf{y} = \begin{bmatrix} \hat{\gamma} \\ \hat{C} \end{bmatrix} \quad \text{and} \quad \mathbf{f} = \begin{bmatrix} \hat{\mathbf{r}} \\ -V_m \hat{\mathbf{r}} \hat{\phi} \end{bmatrix},$$

and we observe that

$$\frac{\partial y_i}{\partial t} = \begin{cases} f_i^1 & C = 0 \text{ and } \gamma_i < \gamma_{eq} \\ f_i^2 & \text{elsewhere} \end{cases}, \quad (21)$$

where

$$\mathbf{f}^1 = \begin{bmatrix} 0 \\ 0 \end{bmatrix} \quad \text{and} \quad \mathbf{f}^2 = \begin{bmatrix} \lambda \left(1 - \frac{\gamma}{\gamma_{eq}}\right) \\ -\lambda \phi V_m \left(1 - \frac{\gamma}{\gamma_{eq}}\right) \end{bmatrix}.$$

Figure 2 shows the discontinuity of the right hand side on the phase plane  $(\gamma, C)$  for the case of a single solute concentration  $\gamma$  and a single precipitate concentration  $C$ .

We can observe that, since the right hand side is discontinuous, it is impossible to state the existence of a solution via Peano's theorem. For this type of problems the Caratheodory existence theorem [14] does not apply either since it considers only discontinuities in the  $t$  variable, while here the discontinuity depends on the solution itself. Thus, we need to resort to Filippov's theory [6] to determine the behavior of the solution at the discontinuities. We also observe that at  $\hat{C} = 0$  we have a finite jump in the right hand side. Figure 3 illustrates, in phase plane, the possible behaviors of the solution at the discontinuity. If we denote with  $\mathbf{n}$  the normal to the hypersurface of

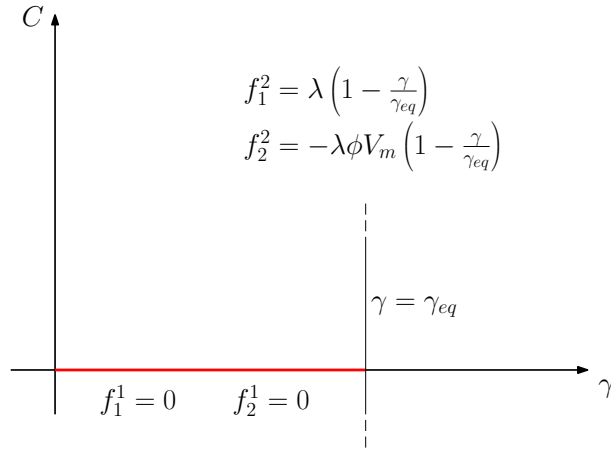


Figure 2: The phase plane associated with the ODE system. The right hand side is discontinuous over the red line, that is  $C = 0$  and  $\gamma < \gamma_{eq}$ .

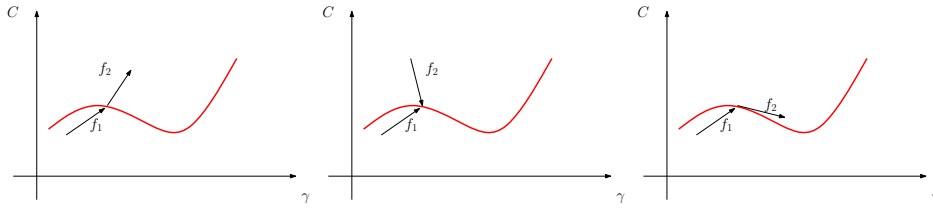


Figure 3: The possible behavior of the solution at the discontinuity in the phase plane. From left to right: crossing, sliding, and tangent.

discontinuity  $\Sigma$  (in our case, it is simply the line  $\hat{C} = 0$ ), once the trajectory reaches the discontinuity we have the following possibilities:

- (a) *crossing solution*, if  $(\mathbf{n}^T \mathbf{f}^1) \cdot (\mathbf{n}^T \mathbf{f}^2) > 0$
- (b) *sliding solution*, if  $(\mathbf{n}^T \mathbf{f}^1) \cdot (\mathbf{n}^T \mathbf{f}^2) < 0$ . In this case the the solution remains on  $\Sigma$ . It means that  $\mathbf{y}(t)$  eventually is a solution of

$$\frac{d\mathbf{y}(t)}{dt} = \mathbf{f}_F(t, \mathbf{y}(t)),$$

where  $\mathbf{f}_F$  is an appropriate vector field which can be computed as a linear combination of  $\mathbf{f}^1$  and  $\mathbf{f}^2$ .

Note that, indeed, in the case of our interest,  $\mathbf{f}^1$  is identically null. It can be shown that once we reach the discontinuity  $\hat{C} = 0$  we have there  $\mathbf{f}_F = [0, 0]^T$ , i.e. the solution will remain constant.

Numerical methods for the integration of DRH-systems can deal with the discontinuity with different approaches, such as step adaptation, or smoothing of the right hand

side. The computational approach used in this work, proposed by [5], is designed to locate with accuracy the points where the transition occurs and check the transversality/sliding conditions stated above through the following steps:

- integration of the ODE outside  $\Sigma$ , in particular, we use an explicit order 2 Runge Kutta method;
- location of the point  $\mathbf{y} \in \Sigma$  reached by a trajectory, and the corresponding time  $t^*$  with an iterative method;
- check of the transversality or sliding conditions;
- in case of sliding motion, integration on  $\Sigma$  with the proper right hand side;

These steps are performed for each degree of freedom during the integration of (20) to achieve a good accuracy and, most of all, to avoid unphysical solutions such as the occurrence of negative concentrations, as we will show in the results.

## 4 Results

We simulate the compaction process of a  $200m \times 120m$  sedimentary layer buried at the depth  $d$ . At the beginning of the simulation  $d = d_0$ , then a sedimentation velocity  $\frac{\partial d}{\partial t} > 0$  brings the domain at a depth  $d(t)$ . We do not model the addition of extra layers due to the progressive burial and the sedimentation acts only as a variation of the boundary conditions. For this reason, the boundary conditions for pressure and overburden are time-dependent. Temperature is a given field and is obtained with a geothermal gradient  $\frac{\partial T}{\partial d}$  and a surface temperature  $T_0$ . The main parameters used for the following simulations are summarized in table 1.

	Value	Unit		Value	Unit
$\beta$	$10^{-8}$	$Pa^{-1}$	$\phi_0$	0.5	-
$d_0$	2000	$m$	$\frac{\partial d}{\partial t}$	100	$m/My$
$T_0$	20	$^{\circ}C$	$\frac{\partial T}{\partial d}$	0.035	$^{\circ}C/m$
$k_0$	$10^{-6}$	<i>Darcy</i>	$g$	9.81	$m/s^2$
$\mu_w$	0.001	$Pa s$	$D$	$1.58 \cdot 10^{-8}$	$m^2/s$
$\rho_w$	1000	$kg/m^3$	$V_m$	0.0226	$m^3/mol$
$\rho_m$	2660	$kg/m^3$	$\rho_d$	2500	$kg/m^3$
$\bar{\rho}$	2500	$kg/m^3$	$\gamma_{eq}$	0.167	$mol/m^3$
$E$	60.1	$kJ/mol$	$\bar{\lambda}$	$8.37 \cdot 10^{-6}$	$mol/(m^3 s)$

Table 1: Physical parameters for the simulation.

We discuss three different initial configurations. In the first case, there is an initial concentration of precipitated mineral in rock in three "bricks" and no mineral dissolved

in water ( $\gamma_0 = 0$ ). In the second configuration, we have no precipitated mineral nor solute at the initial time, but the dynamics is driven by a boundary condition which prescribes  $\gamma$  greater than that of equilibrium at the top of the domain. In the third simulation, we combine the initial concentration of mineral in rock of the first case and the boundary condition on  $\gamma$  of the second simulation.

#### 4.1 Configuration 1: The dissolution of the mineral

In figure 4 the set up for the simulation is shown. We have set for pressure an hydrostatic Dirichlet boundary condition at the top of the domain and at the bottom. The domain is considered as a part of a longer thin layer of rock, lying along the  $x$ -direction, hence no-flux boundary conditions are imposed on the lateral edges. Finally, a Dirichlet condition for the overburden is set at the top and we assume that the bottom of the domain moves downwards with a given, and in our case uniform, velocity.

We solve the problem on a triangular mesh  $50 \times 30$  with time step  $\Delta t = 0.5 \cdot 10^{11} \text{ s} \approx 1.5 \text{ ky}$  to simulate a time span of  $T = 10 \text{ My}$ .

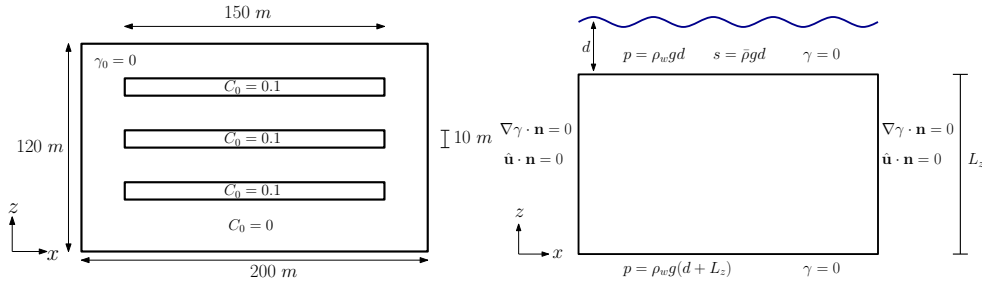


Figure 4: Configuration 1: Numerical setup.

The rock is initially filled with water with no dissolved mineral ( $\gamma_0 = 0$ ). The initial condition for pressure is the hydrostatic pressure and the initial conditions for stress and porosity are computed with some fixed point iterations of the stationary problem. The initial distribution of the precipitated mineral in the rock is sketched in figure 4. Finally,  $\hat{\mathbf{u}}^0 = \mathbf{0}$ .

Since the initial concentration of mineral in water is zero, the precipitated mineral in rock starts to dissolve. Figures 5 and 6 show an increase of  $\gamma$  and a decrease of  $C$ . This behavior lasts as long as there is mineral in rock that can dissolve. Once  $C = 0$ , due to the choice of the boundary conditions, transport and diffusion of the dissolved material in water let the mineral flow out of the domain, leading to a final state where no mineral, either on the rock or in the fluid, is present in the layer.

In figure 7, the porosity is shown, which decreases during the simulation due to the increase of overburden. An higher porosity is obtained, as expected, where the mineral originally present on the rock dissolves. Due to the non-uniform porosity, the domain compacts in a non-uniform way and we can clearly see at the end of the simulation that region in which precipitated mineral dissolves in water compacts more than its neighbor region.

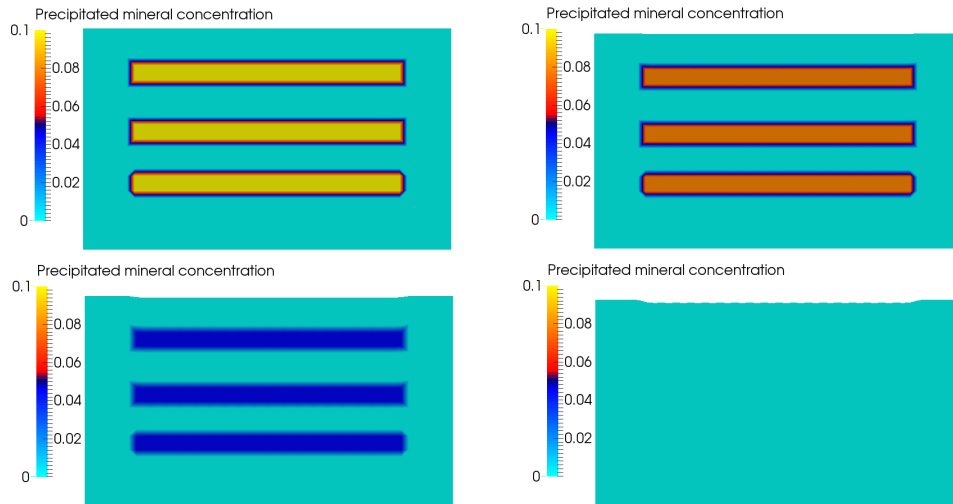


Figure 5: Plot of  $C$  at  $t = 0$ ,  $t = 10/3 My$ ,  $t = 20/3 My$ , and  $t = 10 My$ . The precipitated mineral is decreasing due to  $\gamma < \gamma_{eq}$ , until at the end no mineral is present in the layer.

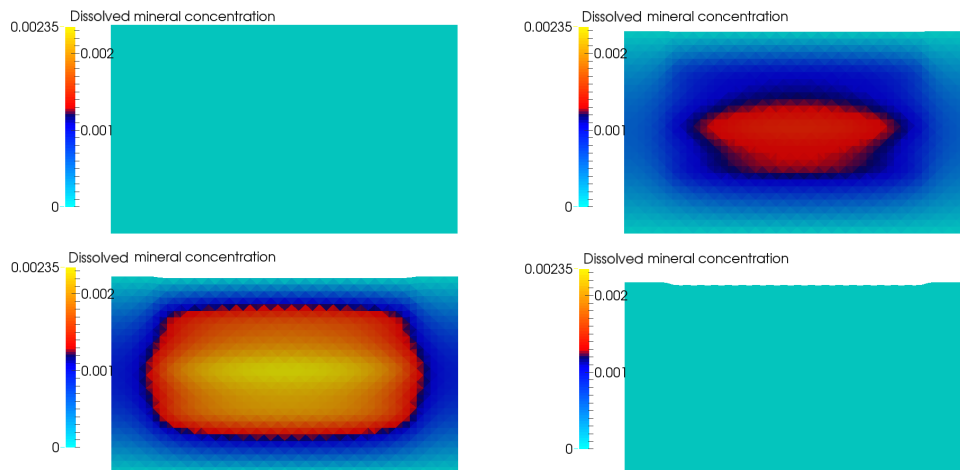


Figure 6: Plot of  $\gamma$  at  $t = 0$ ,  $t = 10/3 My$ ,  $t = 20/3 My$ , and  $t = 10 My$ . The dissolved mineral increases as long as there is material in rock that can dissolve. Finally transport and diffusion let the mineral flow out of the layer.

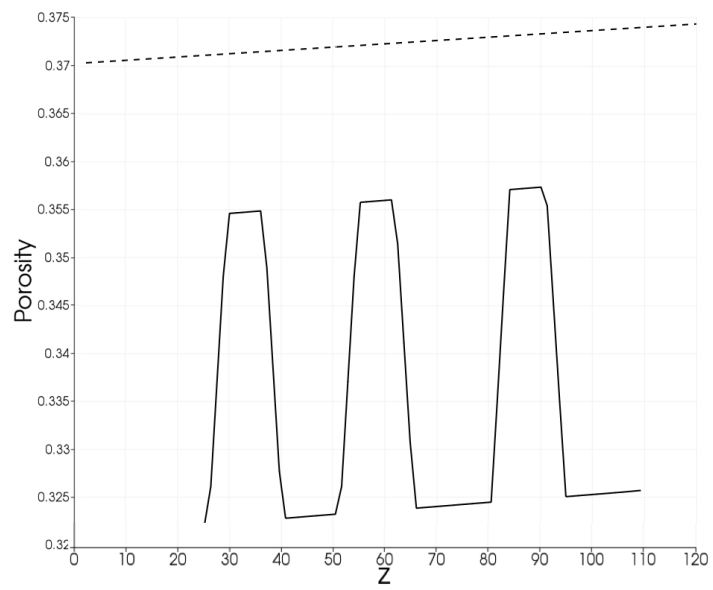


Figure 7: Plot of porosity versus  $z$  at  $t = 0$ ,  $t = 10/3 My$ ,  $t = 20/3 My$ , and  $t = 10 My$ , taken on the vertical line that halves the domain. The dashed and the solid lines represent the initial and the final porosity respectively. Porosity increases in the regions where the mineral on the rock dissolves.

## 4.2 Configuration 2: The precipitation of the mineral

The numerical setup of this simulation is shown in figure 8. The same boundary conditions as in section 4.1 are set, except for that of the dissolved mineral at the top of the domain. Indeed, we set here  $\gamma = 1.5\gamma_{eq}$ .

We solve the problem on a triangular mesh  $50 \times 30$  with time step  $\Delta t = 0.5 \cdot 10^{11} \text{ s} \approx 1.5 \text{ ky}$  to simulate a time span of  $T = 25 \text{ My}$ .

As expected, the mineral in water starts immediately to precipitate at the top of the domain, where its concentration is higher than that of equilibrium, while the solute concentration varies uniformly from the top to the bottom boundary condition (see figures 9 and 10).

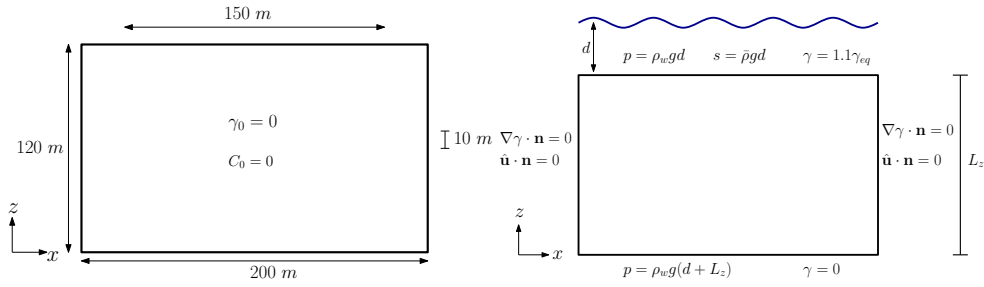


Figure 8: Configuration 2: Numerical setup.

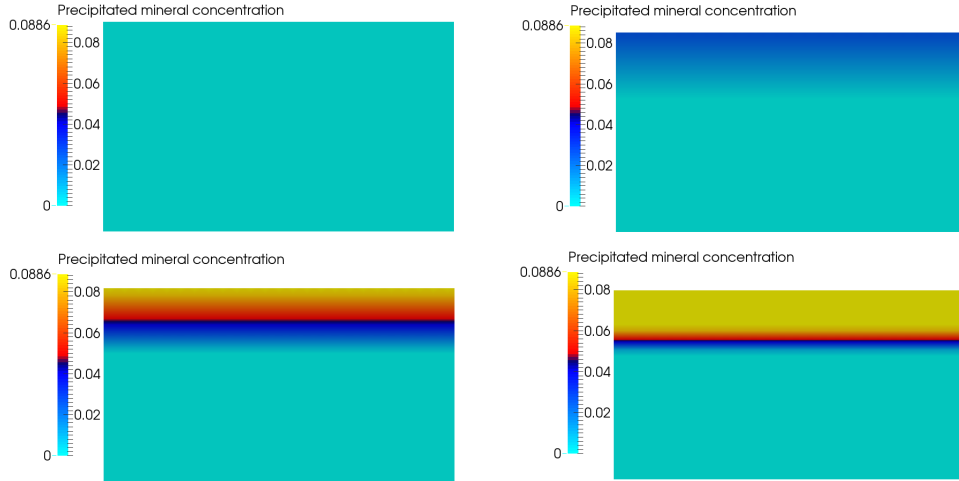


Figure 9: Plot of  $C$  at  $t = 0$ ,  $t = 8 \text{ My}$ ,  $t = 16 \text{ My}$ , and  $t = 24 \text{ My}$ .  $C$  is high at the top, where the mineral in water precipitates.

Also in this case, porosity decreases through the simulation due to the progressive burial. The lower porosity at the top of the domain that we see in figure 11 is caused by the precipitation of the mineral.

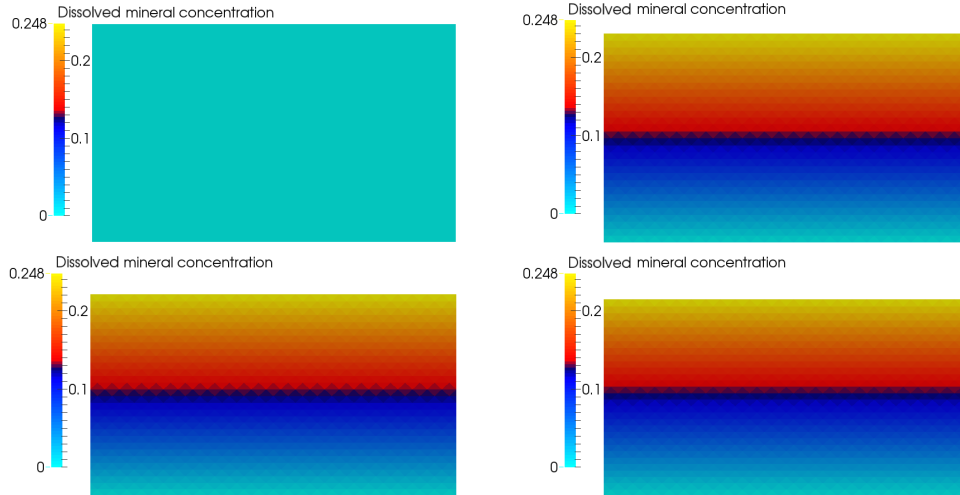


Figure 10: Plot of  $\gamma$  at  $t = 0$ ,  $t = 8 My$ ,  $t = 16 My$ , and  $t = 24 My$ .

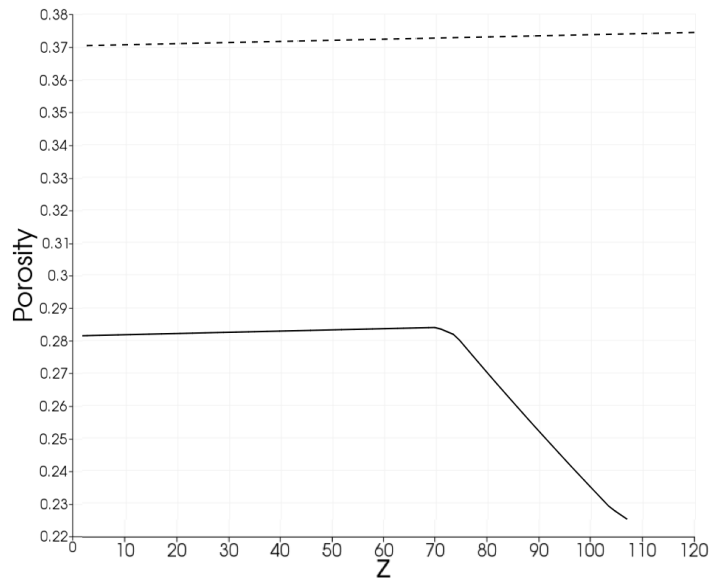


Figure 11: Plot of porosity versus  $z$  at  $t = 0$ ,  $t = 8 My$ ,  $t = 16 My$ , and  $t = 24 My$ , taken on the vertical line that halves the domain. The dashed and the solid lines represent the initial and the final porosity respectively. Porosity is significantly lower at the top of the domain (on the right) due to the precipitated material.

### 4.3 Configuration 3: The general case

The numerical setup of this simulation is shown in figure 12. We have set the same boundary conditions as in section 4.2 and the same initial conditions as in section 4.1.

We solve the problem on a triangular mesh  $50 \times 30$  with time step  $\Delta t = 0.5 \cdot 10^{11} \text{ s} \approx 1.5 \text{ ky}$  to simulate a time span of  $T = 25 \text{ My}$ .

The results obtained are shown in figures 13 and 14.

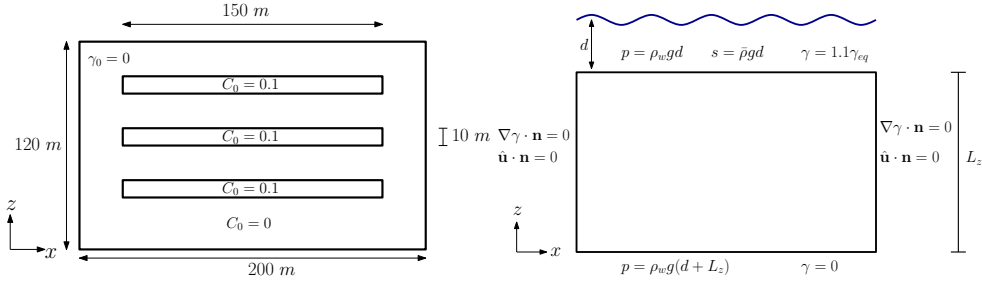


Figure 12: Configuration 3: Numerical setup.

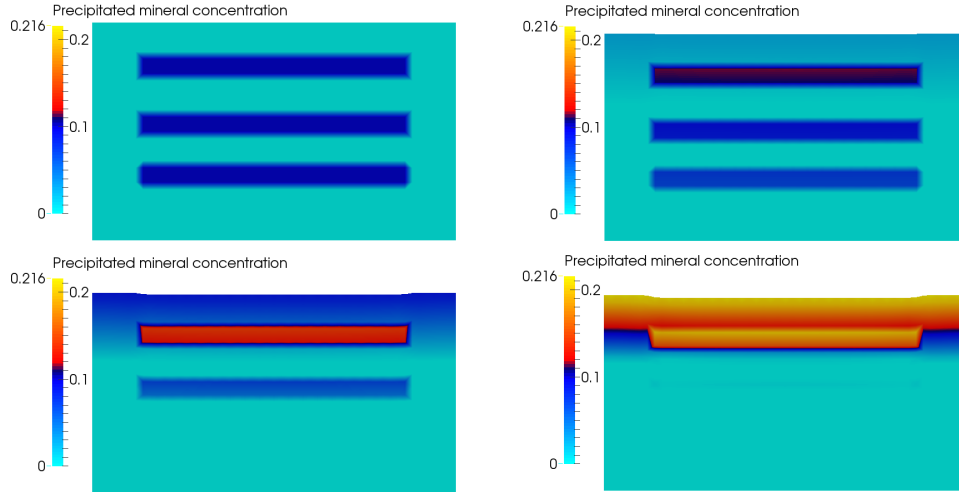


Figure 13: Plot of  $C$  at  $t = 0$ ,  $t = 8 \text{ My}$ ,  $t = 16 \text{ My}$ , and  $t = 24 \text{ My}$ .

Also in this case, see figure 15, porosity is higher where the precipitate concentration was non-zero at the initial time, since the dissolving mineral leaves some void spaces. On the other hand, porosity is lower at the top of the domain, where the mineral precipitates.

Finally, we compare the solutions obtained with two different methods. In figure 16 we shown the concentration of the precipitate obtained with a classical finite element method (dashed line) and that obtained with the *ad hoc* method for ODEs with discontinuous right hand side discussed in section 3 (solid line). We can see that, contrarily to the classical method, the event-driven method prevents  $C$  from becoming negative.

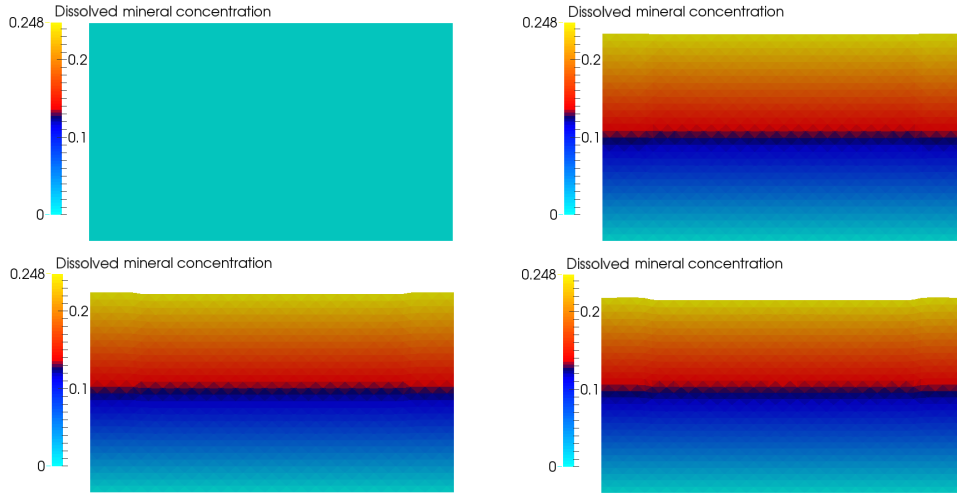


Figure 14: Plot of  $\gamma$  at  $t = 0$ ,  $t = 8 My$ ,  $t = 16 My$ , and  $t = 24 My$ .

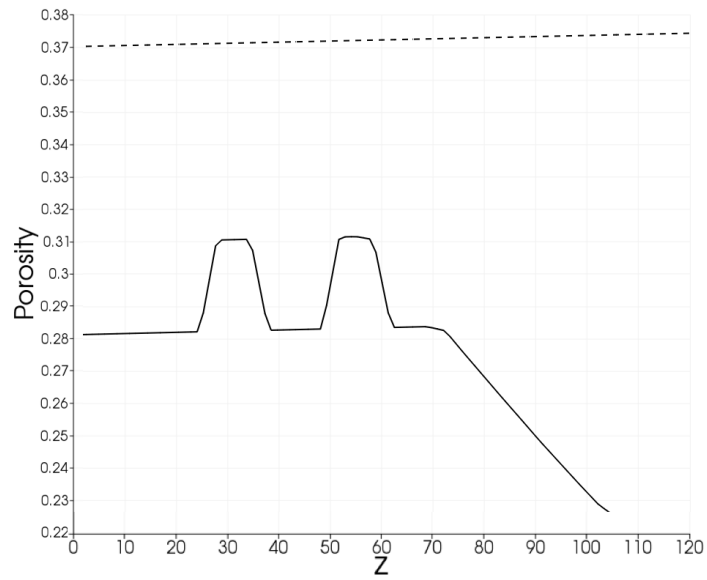


Figure 15: Plot of porosity versus  $z$  at  $t = 0$ ,  $t = 8 My$ ,  $t = 16 My$ , and  $t = 24 My$ , taken on the vertical line that halves the domain. The dashed and the solid lines represent the initial and the final porosity respectively.

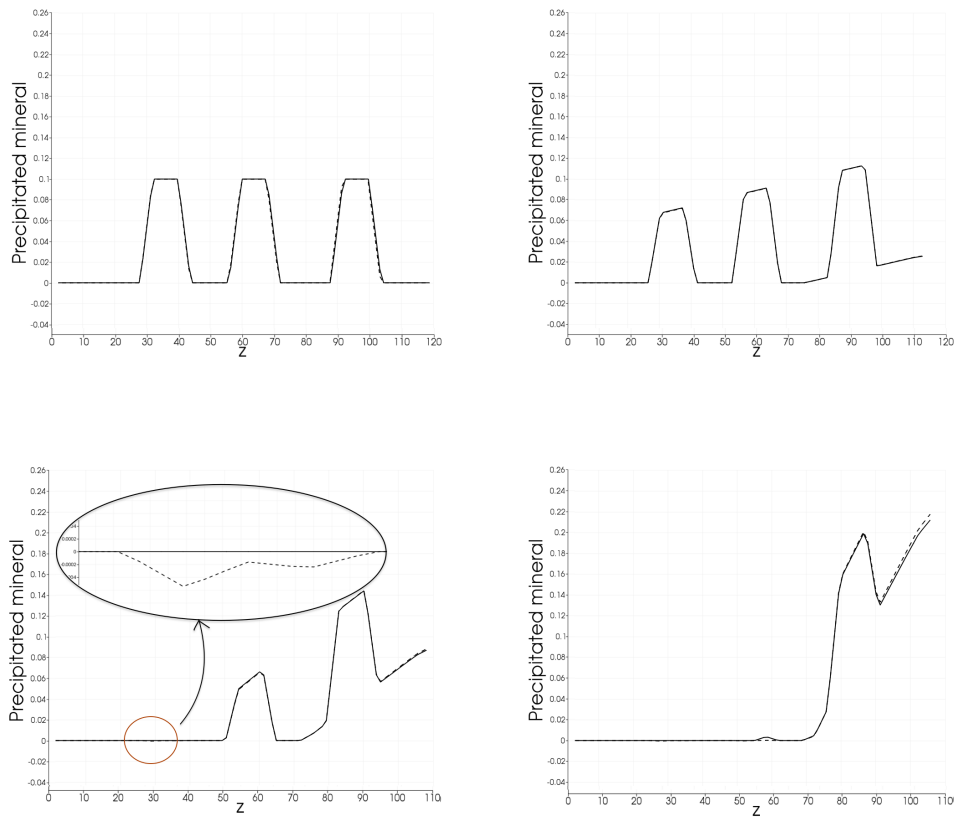


Figure 16: Plot of  $C$  versus  $z$  at  $t = 0$ ,  $t = 8 My$ ,  $t = 16 My$ , and  $t = 24 My$ , taken on the vertical line that halves the domain. The dashed line represents the solution obtained with a classical finite element method, while the solid line is the solution obtained with the *ad hoc* method for ODE with discontinuous right hand side discussed. Notice that the first method allows the solution to become negative, which is nonphysical.

## 5 Conclusion

We have proposed and tested a discretization method for the simulation of compaction in porous media with a particular focus on the numerical treatment of the discontinuous reaction terms that may arise in the modeling of geochemical processes. Even if we are considering a simplified model where only one mineral is allowed to precipitate, dissolve and be advected by the water flow, the results are qualitatively correct and most of all, it is evident that a rigorous treatment of the discontinuity avoids the occurrence of negative concentrations and oscillations. The whole approximation strategy has been developed with the aim of finding a trade-off between accuracy and computational efficiency. However, there is still room for improvement: in particular a more precise assessment of the error introduced by the splittings, will be the subject of future work.

## References

- [1] L. F. Athy. Density, porosity, and compaction of sedimentary rocks. *AAPG Bulletin*, 14(1):1–24, 1930.
- [2] N. Bouillard, R. Eymard, R. Herbin, and P. Montarnal. Diffusion with dissolution and precipitation in a porous medium: mathematical analysis and numerical approximation of a simplified model. *ESAIM: Mathematical Modelling and Numerical Analysis*, 41:975–1000, 2007.
- [3] Z. Chen, R. E. Ewing, H. Lu, S. L. Lyons, S. Maliassov, M. B. Ray, and T. Sun. Integrated two-dimensional modeling of fluid flow and compaction in a sedimentary basin. *Computational Geosciences*, 6:545–564, 2002.
- [4] M.F. Danca. On the uniqueness of solutions to a class of discontinuous dynamical systems. *Nonlinear analysis: real world applications*. in press, doi:10.1016/j.norwa.2009.02.024.
- [5] L. Dieci and L. Lopez. A survey of numerical methods for ivps of odes with discontinuous right-hand side. *Journal of Computational and Applied Mathematics*, 236(16):3967–3991, October 2012.
- [6] A. F. Filippov and F. M. Arscott. *Differential equations with discontinuous right-hand sides*. Springer, 1988.
- [7] A. C. Fowler and X. S. Yang. Dissolution/precipitation mechanisms for diagenesis in sedimentary basins. *Journal of Geophysical Research: Solid Earth (1978–2012)*, 108(B10), 2003.
- [8] C. W. Gear and O. Østerby. Solving ordinary differential equations with discontinuities. *ACM transaction on mathematical software*, 10(1):23–24, 1984.

- [9] K. Kumar, I.S. Pop, and F.A. Radu. Convergence analysis of mixed numerical schemes for reactive flow in a porous medium. *SIAM Journal on Numerical Analysis*, 51(4):2283–2308, 2013.
- [10] R. H. Lander and O. Walderhaug. Predicting porosity through simulating sandstone compaction and quartz cementation. *AAPG bulletin*, 83(3):433–449, 1999.
- [11] D. Lanser and J. G. Verwer. Analysis of operator splitting for advection–diffusion–reaction problems from air pollution modelling. *Journal of Computational and Applied Mathematics*, 111(1–2):201 – 216, 1999.
- [12] J. Nitsche. Über ein Variationsprinzip zur Lösung von Dirichlet-Problemen bei Verwendung von Teilräumen, die keinen Randbedingungen unterworfen sind. *Abhandlungen aus dem Mathematischen Seminar der Universität Hamburg*, 36:9–15, 1971.
- [13] D. L. Ropp and J. N. Shadid. Stability of operator splitting methods for systems with indefinite operators: Advection–diffusion–reaction systems. *Journal of Computational Physics*, 228(9):3508 – 3516, 2009.
- [14] W. Rudin. *Real and complex analysis (3rd ed.)*. McGraw-Hill, 1987.
- [15] M. Wangen. Vertical migration of hydrocarbons modelled with fractional flow theory. *Geophysical Journal International*, 115:109–131, 1993.
- [16] M. Wangen. Two-phase oil migration in compacting sedimentary basins modelled by the finite element method. *International Journal for Numerical and Analytical Methods in Geomechanics*, 21:91–120, 1997.

## MOX Technical Reports, last issues

Dipartimento di Matematica  
Politecnico di Milano, Via Bonardi 9 - 20133 Milano (Italy)

- 06/2015** Perotto, S.; Zilio, A.  
*Space-time adaptive hierarchical model reduction for parabolic equations*
- 09/2015** Ghiglietti, A.; Ieva, F.; Paganoni, A.M.; Aletti, G.  
*On linear regression models in infinite dimensional spaces with scalar response*
- 05/2015** Chen, P.; Quarteroni, A.; Rozza, G.  
*Reduced order methods for uncertainty quantification problems*
- 1/2015** Pini, A.; Stamm, A.; Vantini, S.  
*Hotelling s  $T^2$  in functional Hilbert spaces*
- 2/2015** Menafoglio, A.; Petris, G.  
*Kriging for Hilbert-space valued random fields: the Operatorial point of view*
- 3/2015** Abramowicz, K.; de Luna, S.; Häger, C.; Pini, A.; Schelin, L.; Vantini, S.  
*Distribution-Free Interval-Wise Inference for Functional-on-Scalar Linear Models*
- 4/2015** Arioli, G.; Gazzola, F.  
*On a nonlinear nonlocal hyperbolic system modeling suspension bridges*
- Antonietti, P. F.; Grasselli, M.; Stangalino, S.; Verani, M.  
*Discontinuous Galerkin approximation of linear parabolic problems with dynamic boundary conditions*
- 62/2014** Andrà, C.; Parolini, N.; Verani, M.  
*Using gambling simulators to foster awareness about gambling risks*
- 61/2014** Taffetani, M.; Ciarletta, P.  
*Elasto-capillarity controls the formation and the morphology of beads-on-string structures in solid fibres*